Solar Energy Materials & Solar Cells 292 (2025) 113803

Contents lists available at ScienceDirect

Solar Energy Materials and Solar Cells

journal homepage: www.elsevier.com/locate/solmat

Rheological study on xylitol crystallization for its use as phase change material: analytical and statistical analysis

Miguel Navarro [a,*], Zeus Gracia [b], Jesús Asín [b], Ana Lázaro [a], Marta Martí [a], Mónica Delgado [a]

[a] Aragón Institute for Engineering Research (I3A), Thermal Engineering and Energy Systems Group, University of Zaragoza, Agustín de Betancourt Building, C/María de Luna 3, 50018, Zaragoza, Spain

[b] Department of Statistical Methods, University Institute of Mathematics and Applications-IUMA, University of Zaragoza, 50009 Zaragoza, Spain

ARTICLE INFO

Keywords:
LHTES
Crystallization
Xylitol
Classical nucleation theory
Cumulative distribution function

ABSTRACT

In a global context in which decarbonization of society is wanted through the use of renewable sources, energy storage plays a fundamental role. Among the different forms of energy storage that exists, this work focuses on latent heat energy storage (LHTES) for medium-low temperatures, between 70 °C and 120 °C. Xylitol, a sugar-alcohol, is a promising phase change material (PCM) due to its low cost, low corrosivity, high latent heat (240 J/g) and a melting temperature of 92 °C. However, its use as PCM is hindered by a high degree of supercooling and a low crystallization rate. To address these challenges, this work used a seeding and shearing technique to trigger crystallization. Rheological experiments were performed to monitor viscosity changes during crystallization, in order to study the crystallization induction time. The systematic analysis included the effects of temperature (70–90 °C), shear rate(1-100s^{-1}), and seed crystal size (300–400 μm and 600–700 μm). Key results show that temperature is the most dominant factor. The shortest induction time at 70 °C was found at 10s, increasing to 1500s at 90 °C. Increasing seed size and reducing the rheometer gap also shortened induction times, while shear rate had minimal influence, likely due to non-uniform shear during the test. For practical applications, operating at 80 °C is recommended to balance induction time and energy loss due to supercooling. Optimizing shear-triggered mechanism, such as stirred tanks designs, can improve crystallization controllability.

1. Introduction

On the road to the decarbonization of society, energy storage is essential to minimize the impact of the mismatch between demand and energy generation due to the intermittent nature of renewable energy sources, such as solar or wind. Different technologies can be used for energy storage, such as batteries or pumped hydro, but this work focuses on thermal energy storage, specifically latent heat thermal energy storage, or LHTES. LHTES uses the phase change of the material, called phase change material (PCM), to store and release thermal energy. LHTES can store more energy per unit of volume than sensible heat thermal energy storage for a given small temperature range. For example, given a temperature range of 15 °C, water can store 17 kWh/m^3, and xylitol can store more than 100 kWh/m^3 from 85 to 100 °C.

Several materials can act as PCMs, such as paraffins or molten salts. Sugar alcohols (SA) are materials with high potential for thermal energy storage at low-to-medium temperatures. SAs are organic materials that possess high latent heat and densities compared with other PCMS. They are also of natural origin, sustainable and cheap [1,2]. However, most SAs suffer from supercooling and have low crystallization rates, which can hinder their potential to act as PCMs in a LHTES system [2,3]. Supercooling is usually considered a drawback, as it prevents the discharge of the stored energy at the phase change temperature. However, supercooling can be beneficial in instances where the energy stored is not needed, but the PCM is approaching the phase change temperature due to the thermal losses of the system.

Several studies in the literature deal with the activation of crystallization by different techniques. Englmair et al. [4] use an activation device to trigger sodium acetate trihydrate crystallization by adding solid seeds to the supercooled liquid. Anish et al. [5] do not use any activation system to trigger crystallization in a compact spiral coil heat exchanger as a thermal energy storage system in which xylitol reaches a low temperature. In Coccia et *al.* [6], a mechanical device is used manually to trigger xylitol crystallization in a solar cooker to stabilize the temperature of the liquid placed inside the cooker. They reported

* Corresponding author.
E-mail address: miguel.navarro@unizar.es (M. Navarro).

https://doi.org/10.1016/j.solmat.2025.113803
Received 4 March 2025; Received in revised form 2 June 2025; Accepted 19 June 2025
Available online 25 June 2025

Nomenclature

Variables

A_{surf}	Kinetic parameter [Pa · m^{-3}]
B_{surf}	Metastable zone parameter [K^3]
G	Crystal growth [m/s]
J	Nucleation rate [$m^{-3} \cdot s^{-1}$]
k_B	Boltzmann constant [$m^2 \cdot kg \cdot s^{-2} \cdot K^{-1}$]
P(t)	Cumulative probability
T	Temperature [K]
t	Time [s]
t_{ind}	Induction time
t_g	Time delay between the start and detection of crystallization
T_m	Melting point [K]
T_{sup}	Supercooled temperature [K]
t_{ind}	Induction time [s]
V	Volume [m^3]

Greek symbols

α_{crist}	Minimum solid fraction
ΔG^*	Free activation energy [kJ/mol]
φ	Solid fraction
φ_{max}	Maximum packing fraction
μ_m	Suspension medium viscosity [Pa·s]
μ_{susp}	Suspension viscosity [Pa·s]
$[\mu]$	Intrinsic viscosity

Abbreviations

ANOVA	Analysis of Variance
GLM	General Linear Model
LHTES	Latent Heat Thermal Energy Storage
PCM	Phase Change Material
SA	Sugar Alcohol

induction times of 15–20 min after using the activation device, but no seed was added.

Among SAs, xylitol has very high potential as PCM, as it shows relatively high phase change enthalpy with a melting point of 92 °C, showing only one morphism at the temperature range studied and better thermal endurance [1–4]. Xylitol was discovered in 1891 and is used as a sugar substitute with the European Union code number E967. Xylitol is a 5-carbon polyol, produced normally from xylose, which can be found in agricultural, agro-industrial and forestry residues [5], like birch trees and other hardwoods. Xylose is usually submitted to a hydrogenation process to obtain xylitol, although other production techniques are being studied, such as fermentation [6,7].

Xylitol has a high phase change enthalpy (240 J/g) and a phase change temperature below 100 °C (92 °C) and a polymorphism that appears at 61 °C [8], which has not been reported again in later literature. Xylitol also suffers from supercooling and low crystallization rate. Some techniques can be used for the triggering of xylitol crystallization, such as bubbling [9,10], shearing and seeding [4,11] or adding additives [12]. This work will use the technique of shearing and seeding in the same setup as the one used by Delgado et al. [4]. Xylitol has lower phase change enthalpy than erythritol or mannitol. However, the stable undercooling, the lower phase change temperature and only having one polymorphic form in the working range makes xylitol a promising PCM among other sugar alcohols.

Even though the stability of the phase change materials is an important topic, the stability of xylitol is not well studied [3]. There are studies on different sugar alcohols, like erythritol or d-mannitol. [3,13,14]. Diarce et al. [3] studied the thermal endurance of xylitol, demonstrating that xylitol maintained 95 % of its phase change enthalpy after being maintained at a temperature 28 °C higher than its melting point for 30 days. In contrast, other sugar alcohols show an important decrease in their melting enthalpy after only one day of testing.

Crystallization is the process by which solid crystals appear in a liquid sample, in some materials being the phase change from liquid to solid state. This phenomenon can be broken down into two stages: nucleation and crystal growth. Nucleation is the process by which nuclei of crystalized material appear in the liquid, and it represents the emergence of nuclei (crystals) in the liquid. Nucleation can be divided into two categories: primary and secondary nucleation.

Primary nucleation occurs when crystals appear spontaneously in the liquid material, e.g. due to a locally high solute concentration within the mixture [15]. Secondary nucleation starts from the appearance of new crystals in the mixture from pre-existing crystals. This can be caused by the shear action of the fluid on the crystals (which can cause a separation of the outer layer of the crystal); or even the complete or partial break-up of a crystal due to collisions between crystals or due to collisions of the crystals with elements of the system, such as the stirrer blades or the walls [16].

Crystallization is a stochastic process [17]. As such, using the cumulative probability of the detection time of crystallization seems to be a technique used in literature to study nucleation from a stochastic point of view [18,19].

In this work, crystallization is studied indirectly by measuring the viscosity of the solid-liquid mixture of the phase change as crystallization is related to the viscosity because of the solid fraction. The relationship between the solid and liquid fractions is well studied, and several formulas relate them, like a Power Law or the Krieger-Doherty formula [20,21]. Crystallization will be studied by calculating the induction times. Different techniques are used to calculate the induction times of crystallization of a material, like light refraction [22] or temperature evolution [10]. However, the techniques used are very system-dependent, and in this work, neither of them can be used. As the viscosity vs time curves are obtained for each test, a similar approach as in Navarro et al. [11] is used. The induction time is calculated by calculating the intersection between the baseline and the tangent at the inflexion point of the viscosity curve. Similarly, classical nucleation theory's study of induction times does not explain the stochastic nature of crystallization. Therefore, some studies propose the calculation of the cumulative probability of induction times to study the nucleation of a process [18,19,22].

This work aims to understand the influence of different factors in xylitol crystallization by shearing and seeding. Although crystallization is a system-specific process, meaning that crystallization in the rheometer will be different than in a real energy storage system, studying crystallization in a rheometer can provide valuable insights into the variables that affect crystallization in any type of system. Thus, the results of this work can help in the development of a thermal energy storage system based on a stirred tank with a coil, a robust system already used as an energy storage system.

2. Materials and methods

2.1. Xylitol

Xylitol (CAS number 87-99-0) at 99 % purity from Alfa Aesar is used in this study. Xylitol can form only one form within the temperature range, a stable orthorhombic form at 92 °C [8].

Xylitol seeds used in this study were obtained by sieving fresh, bulk xylitol. Two different seed sizes were used in this study. Smaller seeds had a diameter between 300 and 400 μm, and bigger seeds had a

diameter between 600 and 700 μm. These seeds were obtained using standard test sieves. For the small seed size, particles that passed through the 400 μm sieve but were retained on the 300 μm sieve were selected. Similarly, for the large seed size, particles that passed through the 700 μm sieve but were retained on the 600 μm sieve were chosen.

2.2. Rheological measurements

This work will study the influence of temperature, shear, seed size and mass in xylitol crystallization. The equipment used for the study was a controlled stress rheometer from TA Instruments, model AR-G2. A Peltier plate was used as the temperature control of the sample, and the geometry selected was a 40 mm parallel plate geometry. As the measured temperature is the Peltier plate temperature and not the sample temperature, waiting period is required to allow thermal equilibrium between the Peltier plate and the sample. However, as the geometry is not heated, a small temperature gradient arises unavoidably. As stated by Navarro et al. [11], xylitol would increase its temperature to 90–92 °C after the triggering of crystallization in a tank. In this study, however, the focus is on the start of the crystallization, and therefore, the influence of recalescence on crystallization should be minimized.

The plate geometry was selected as the mechanical stirring of the plate geometry provokes not only shearing, but also collisions (mainly crystal-crystal and crystal-geometry collisions), which can influence crystallization of xylitol.

Before performing the rheometer tests, the amount of solid xylitol required for the test is prepared in a container, and a syringe is filled with liquid xylitol. At the beginning of each day, the oven is heated to 105 °C, and the syringes are placed inside to preheat them before use in the tests. The containers and syringes contain half of the material used in each test, which is dependent on the distance between the Peltier plate and the geometry of the rheometer, referred to as the gap selected for the experiment.

Assuming that the volume follows a cylindrical shape, the total volume of xylitol when the gap is 600 μm, given that the geometry has a radius of 20 mm, is 0.75 ml, corresponding to 1.09g. In the case of 1000 μm, the volume is 1.25 mL, corresponding to 1.75g. These values have been calculated assuming a density of 1.45 g/ml.

The different factors and levels are shown in Table 1: five different temperatures, three different shear rates, and two different seed sizes, gaps and number of seeds. Each variable level selected is justified below. Navarro et al. [11] explained how the supercooling reduced the total energy available, which added to the high viscosity of xylitol at low temperatures (3.07 Pa s at 70 °C [2]), means that it is not recommended to use xylitol with high supercooling (xylitol is analyzed in the 70–90 °C temperature range and not at lower temperatures). The shear rates are selected as $10s^{-1}$ is the shear used in the same setup of Delgado et al. [4]; and the other two shear rates are one order of magnitude higher and lower. The seed size chosen is the same as in the Delgado et al. study [4], and double the size of the seed. The gap used is the same as in this study, and a bigger gap is used to accommodate the largest seed size chosen. Both the seed size and the gap are related to crystal-geometry collisions, which can have a great impact on crystallization. As the movement of the crystals in the melt is chaotic, and the fact that this study focuses on the initial stage of crystallization, when only a few crystals are present, the effect of the seed size or the gap could provide some insights into the relevance of collisions in xylitol crystallization. Higher gaps combined with smaller seeds could result in fewer crystal-geometry collisions in this geometry, which will influence induction time if such collisions are a relevant mechanism in xylitol crystallization. Seed size is also related to crystal-crystal collisions. Also, the gap is closely associated with sample mass due to the changes in density because of the temperature. Consequently, the tests at 90 °C with a 600 μm gap will have higher mass than those at 70 °C with the same gap.

Table 1
Factors and levels for xylitol tests.

Temperature [°C]	Shear rate [s^{-1}]	Seed Size [μm]	Gap [μm]	Number of seeds
70	1	300–400	600	1
75	10	600–700	1000	
80	100			
85				
90				

On the other hand, for the cumulative probability analysis of the crystallization, it is necessary to repeat one of the repetitions many times [18]. In this case, the levels 70, 80 and 90 °C (supercooled temperature) have been chosen, as both in the literature and the analysis, it is observed that temperature is the most determining factor.

The procedure for carrying out the rheometer tests is as follows.

1. Prepare a syringe with half of the needed xylitol.
2. Set the test temperature
3. Raise geometry to 120 000 μm
4. Load the contents of the canister into the Peltier.
5. Increase the temperature to 120 °C and wait 15 min to ensure that the xylitol is fully melted. Change the gap to 1000 μm after 1 min to preheat the geometry.
6. Decrease the temperature to the temperature chosen for the test and wait 5 min.
7. Raise the geometry, add the seed and the other half pre-heated xylitol to the loaded xylitol.
8. Adjust the gap
9. Start the test

The end of the test is given by two different cases. In the first case, the completely crystallized xylitol prevents the geometry from continuing to rotate, and very high or even negative viscosity values are recorded. In the second case, the xylitol is detached from the Peltier plate, causing an abrupt drop in viscosity.

2.3. Induction time definition

The induction time in a process refers to the period from the start of the process until a significant level of change or activity is reached. It represents the time required for the first measurable effects or transformations to occur in the system. The calculation of the induction time depends on the variable selected to study crystallization. Commonly, the reflectivity of the material is used as a method to measure the crystallization state of the material [22]. Other methods include using a Raman spectrometer or the light transmissivity of the mixture.

In this case, crystallization is measured as a function of viscosity; as viscosity is related to the solid phase of a mixture, which means that viscosity is related to crystallization. In the case of xylitol, induction times are assumed to be dependent on the initial xylitol temperature (supercooling), the shear rate, seed size and gap used for promoting the crystallization. Obtaining different induction times at different variable levels will allow for a statistical analysis.

To define the induction time, the viscosity curve will be analyzed as a function of the time obtained from the rheometer. There are several methods to determine the induction time.

1. Exceeding a set limit: Determination of the induction time by exceeding a predefined threshold [10].
2. Intersection between the baseline and the tangent of the curve: Calculation of the induction time through the intersection between the baseline and the tangent of the curve at the inflection point [11].
3. Offline Changepoint detection methods: Identification of the induction time using statistical techniques of change detection in the data [23].

To define the induction time, the viscosity curve obtained from the rheometer is analyzed as a function of time. Similar to the study by Navarro et al. [11], the induction time is calculated by the intersection of the baseline and the tangent of the curve of the measured property; in the case of the study mentioned above, it is the temperature, and in this work, it is the viscosity.

In this approach, a baseline representing the initial or steady state of the system is plotted, and the tangent of the curve at the inflection point is calculated. The induction time is determined as the point of intersection between the baseline and the tangent of the curve. This method allows a more accurate measurement of the time at which the significant change is initiated. Fig. 1 shows a graphical representation of the method explained.

2.4. Nucleation rate measurement

The nucleation rate of crystallization refers to the number of crystals that appear in a solution in a timeframe. As such, the nucleation rate can be used to compare how different test conditions affect crystallization.

2.4.1. Classical nucleation theory (CNT). Relationship between induction time and nucleation rate

For the measurement of the nucleation ratio, different techniques are available. It can be measured directly by using crystal counting techniques on an image of a surface of the nucleating system, or it can be measured indirectly by studying properties that are affected by the nucleation process, such as changes in transmissivity or increasing solution temperature [22,24].

Classical Nucleation theory proposes formulas to calculate the nucleation rate, defined as the number of nuclei created per unit of liquid value and second [*/m^3·s]. For example, nucleation rate can be assumed to follow an Arrhenius behavior following equation (1) [25]:

$$J = A \cdot \exp\left(\left[-\frac{\Delta G^*}{k_B \cdot T}\right]\right) \tag{1}$$

Where J is the nucleation rate, ΔG^* is the free activation energy and k_B is the Boltzmann constant.

Results obtained by classical nucleation theory can differ significantly from experimental results, sometimes by up to several orders of magnitude. In general, these results are usually not quantitatively accurate but may be acceptable in terms of their qualitative validity [25].

It is possible to relate the induction time to the nucleation rate. Kashchiev [26] defined a formula which relates induction time to the nucleation rate, shown in equation (2). Induction times may vary depending on the measurement method employed. Therefore, nucleation ratios will also depend on the measurement method. This underscores the importance of using a consistent and appropriate approach to nucleation ratio measurement depending on the objectives of the study and the characteristics of the crystallization system.

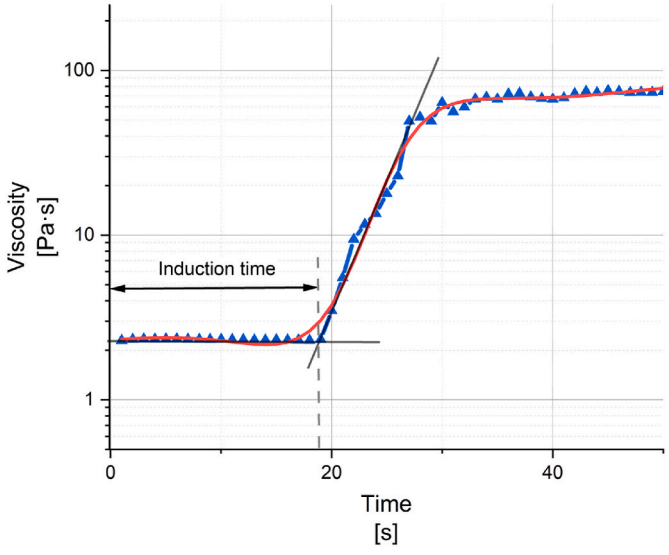

Fig. 1. Induction time definition in a viscosity-time curve.

$$t_{ind} = \sqrt[4]{\frac{\alpha_{crist}}{\frac{\pi}{3} \cdot G^3 \cdot J}} \rightarrow J = \frac{\alpha_{crist}}{\frac{\pi}{3} \cdot G^3 \cdot t_{ind}^4} \tag{2}$$

Where J [*/m^3·s] is the nucleation rate, G [m/s] is the crystal growth, t_{ind} [s] is the induction time, and α_{crist} is the minimum solid ratio detected by the measurement system. The crystal growth G is taken as dependent on temperature as calculated in Zhang et al. [2].The solid fraction should be very small, so the Krieger-Dougherty formula [15], shown in equation (3), is used to calculate the solid fraction value.

$$\mu_{susp} = \mu_m \cdot \left(1 - \frac{\varphi}{\varphi_{max}}\right)^{-[\mu]*\varphi_{max}} \tag{3}$$

where μ_{susp} is the viscosity of the suspension, μ_m is the viscosity of the suspension medium, φ is the solid volume fraction in the suspension, φ_{max} is the maximum packing fraction and [μ] is the intrinsic viscosity of the system. The values of φ_{max} and [μ] depend on the type, shape and size of the dispersity of the suspended particles.

To calculate the solid fraction using equation (3), both the viscosity of the medium and the viscosity of the emulsion are needed. In the case of this work, the value of the emulsion viscosity will be taken as the value of the xylitol viscosity at the induction time.

2.4.2. Classical nucleation theory. Nucleation rate model as a function of temperature

The modelling of the nucleation rate assumes dependence of nucleation rate with supercooling, following Piquard et al. [10] assumptions. This model is born from the combination of Mullin [27] and Mersmann [28] equations, by which equation (4) is derived:

$$J = \frac{A_{surf}}{\mu(T_{sub})} \cdot \exp\left(\frac{-B_{surf}}{T_m \cdot (T_m - T_{sup})^2}\right) \tag{4}$$

Where T_m is the melting temperature, T_{sup} is the temperature of the supercooled liquid, μ is the viscosity of the material at the supercooled temperature, and both A_{surf} and B_{surf} are empirical constants related to the intensity of the mechanism and the metastable zone, respectively. To complete the model, A_{surf} and B_{surf} should be obtained for each test condition by using the nucleation rates calculated from equation (2).

As the formula is exponential, a linearization of the equation could improve the fit of the equation and make it easier to obtain both A_{surf} and B_{surf}, as suggested by Piquard et al. [10]. By doing so and rearranging the initial equation, equation (5) is reached.

$$T_m \cdot (T_m - T_{sup})^2 \cdot \ln(J \cdot \mu(T_{sup})) = T_m \cdot (T_m - T_{sup})^2 \cdot \ln(A_{surf}) - B_{surf} \tag{5}$$

For equation (5) to be linear, a variable change is necessary. If $T_m \cdot (T_m - T_{sup})^2$ is considered as X, the equation is akin to a straight line, where ln(A) is the slope and B is the independent term; as shown in equation (6)

$$X \cdot \ln(J \cdot \mu(T_{sup})) = X \cdot \ln(A_{surf}) - B_{surf} = Y \sim y = mx + c \tag{6}$$

Once A and B are obtained from the linear fitting, they are used in equation (4) for the calculation of different nucleation rate values at different temperatures.

It is important to note that the usual nucleation rate equations (equation (1) and equation (4)) can lead to different results, although they both start from the Classical Nucleation Theory. Equation (1) indicates that the nucleation rate increases with temperature, while from equation (4), it can be seen that the nucleation rate increases to a

maximum and then decreases as the model approaches the melting temperature. This discrepancy may be because these equations model different processes: equation (1) models a nucleation process in a supersaturated solution, while equation (4) models a supercooling process. Usually, the effect of temperature is not clear as it may change depending on the system and its specific work conditions [25].

2.5. Statistical analysis

For the statistical analysis, a generalized linear model with a Gamma log-link function was used, as detailed in section 3.3. This type of analysis was performed as other types of analysis, such as ANOVA, do not perform well due to the stochastic nature of the induction times.

The factors shown in Table 1 were taken for the statistical model as explanatory variables: temperature, shear, gap and seed size. Within the factors, temperature was modeled using a third-degree polynomial, while only a first-order has been considered for the rest of the factors. The statistical model estimates coefficients for each variable while accounting for the effects of the others. Their significance is assessed using t-statistics, where larger absolute values indicate stronger evidence against the null hypothesis of no effect. Given the log-link function of the model, the exponential of the coefficients is the scale of the original response (i.e., induction time). However, because temperature was modeled using a third-degree polynomial, the individual polynomial coefficients do not directly correspond to interpretable effects in the original temperature units.

The statistical analysis was done using R (v4.4.1; RRID:SCR_001905) and the standard libraries.

2.6. Cumulative distribution function

In a crystallization process, the induction time can vary significantly and be different in each test since crystallization is a random process and, on many occasions, it is not possible to fully explain the differences that exist in the nucleation time when tests are carried out under the same conditions. It is for this reason that induction times can be studied by calculating the cumulative probability of crystallization, where there is always a minimum induction time, where the probability of nucleation is zero, and a maximum nucleation time, where the probability of crystallization is 100 %.

This variation in induction times can be explained if suspension formation depends on a single nucleation event. This event depends on the probability of nucleus formation in a given time. It is assumed that the distribution of induction times follows a Poisson distribution [29], so the probability of nucleus formation can be defined as:

$$P(t) = 1 - \exp\left(-J \cdot V \cdot (t - t_g)\right) \tag{7}$$

Where J is the nucleation rate, V is the volume of the system, and t_g is the time delay for crystal detection calculated as the subtraction between the start of the experiment and the time it takes to detect crystals [22,29].

By carrying out multiple tests under identical conditions, it is possible to obtain the cumulative distribution function of induction times. From this function, the nucleation rate can be calculated using equation (7). This approach is one way of dealing with the variability of crystallization and provides a more realistic perspective by recognizing that induction times can vary considerably in a crystallization process.

3. Results and discussion

For the results, it is assumed that the induction times and the nucleation rate are dependent on temperature. As such, induction time and nucleation rates graphs have temperature as the X-axis variable. The results shown in sections 3.1 and 3.2 are grouped first by shear and second by gap and seed size.

All the graphs show all the data, and the different colors and shapes are used to identify the different cases.

3.1. Induction time

The induction times calculated for the tests varying the experimental conditions detailed in Table 1 are shown in Figs. 2 and 3. The induction times plots show a clear upward trend at low supercooling, meaning that lower supercooling leads to higher induction times. There are a lot of variances between gap and seed size (Fig. 2) and shear (Fig. 3), and no conclusions can be drawn definitively.

3.2. Classical nucleation theory modelling

The experimental nucleation rates are obtained from the Kaschiev formula [26], shown in equation (3), using the induction times calculated and shown in the previous section. These nucleation rates are represented by the points in both Figs. 4 and 5. The results are grouped in the same way as the previous section, and each nucleation rate corresponds to one specific induction time.

For the classical nucleation theory results, first, the A and B parameters are calculated by using the methodology discussed in section 2.4.2. The Origin software from OriginLab was used for the linear fitting, and both the R-squared and standard deviation were calculated for the linear fitting. As in the previous section, the data is also filtered by shear and gap/seed size. The different slopes and intercepts parameters are shown in Table 2, with the standard deviation and the R-squared of the fitting. The slope is related to the A_{surf} parameter, while the intercept is related to the B_{surf} parameter.

Figs. 4 and 5 show the results of the experiments and the modelling, both from the classical nucleation model using equation (4). The colored area is obtained by substituting the values given by the fit, shown in Tables 2 and in equation (4). It can be seen that, while in Fig. 4 there are some differences between tests at different gaps and seed sizes, the influence of shear shown in Fig. 5 is not very clear.

The variability observed in the tests at different shear rates may be due to the methodology followed in this work. When the seed is in the supercooled xylitol sample, it is placed in the center, and then the second half of the xylitol is loaded with a syringe. Because of the type of geometry used, flat plate geometry, the shear is variable along the radius, and the test shear is observed at the edge of the geometry, which causes the seeds moving through the supercooled xylitol sample to be sheared

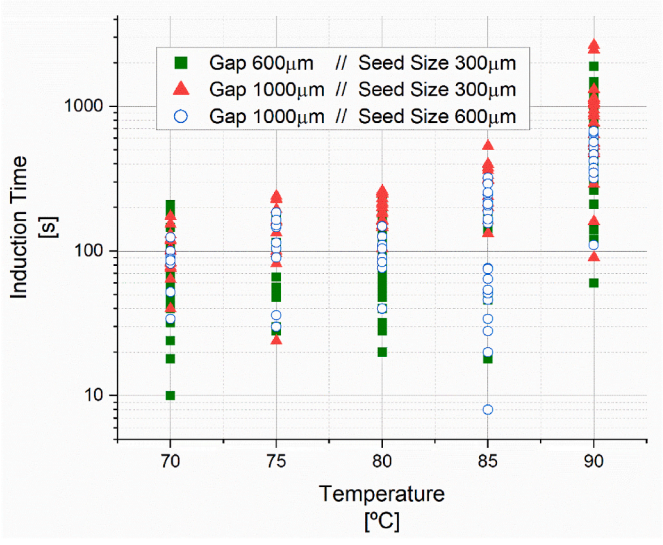

Fig. 2. Induction time grouped by gap and seed size for xylitol studied in a rheometer.

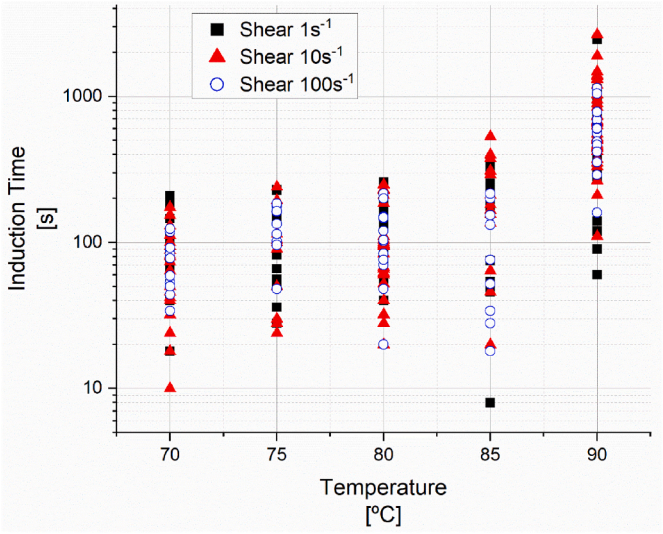

Fig. 3. Induction time grouped by shear for xylitol studied in a rheometer.

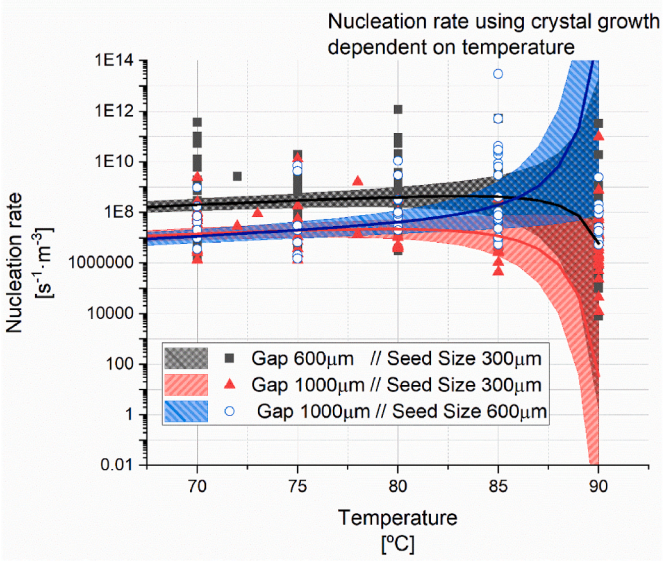

Fig. 4. Nucleation rate for different gaps and seed sizes.

at different shear rates. On the other hand, seed placement is difficult because the loading of the molten xylitol with the syringe causes the initial seed to move, making it difficult to place and preventing the seed from being fully centered.

For both Figs. 4 and 5, the model seems to work better at higher supercoolings, and at temperatures near the melting point, the model range seems to not work properly. Also, the great variance in the nucleation rates calculated from the Kaschiev formula [26], shown in equation (3), is not shown in the nucleation rate using the adapted model [10], which follows equation (4). These problems make it difficult to get insights on the differences made by the different crystallization conditions. To explore the differences between the crystallization conditions, an ANOVA analysis is performed on the induction times calculated in the previous section.

3.3. Statistical analysis

To explore the data, the box plot of induction time by the different factor quantities has been made (Fig. 6), along with the density probability plot of the induction times by temperature factor, shown in Fig. 7.

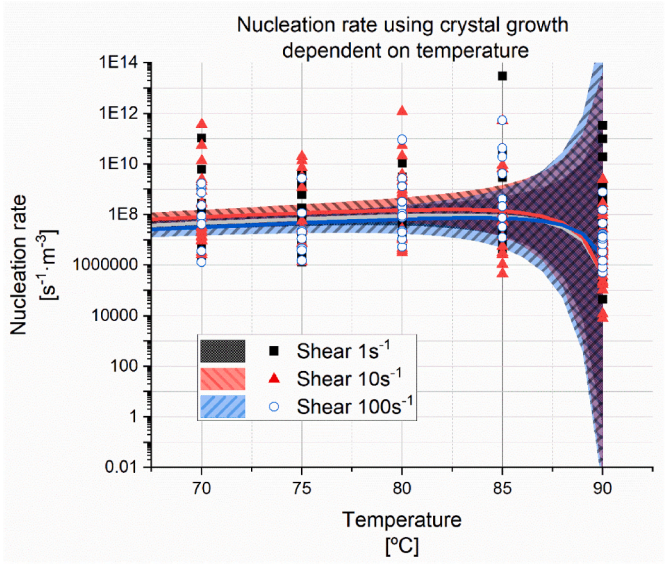

Fig. 5. Nucleation rate for different shear rates.

Table 2
Slope and Intercept parameters of the linear fitting for the nucleation rate modelling.

Data group	Slope [ln (A_{surf})]	Intercept [B_{surf}]	R-squared
Gap 600 µm Seed 300 µm	20.34 ± 0.36	−10865.97 ± 30742.19	0.96
Gap 1000 µm Seed300 µm	17.81 ± 0.35	−30807.77 ± 28723.44	0.97
Gap 1000 µm Seed 600 µm	17.21 ± 0.42	35664.71 ± 33464.03	0.97
$1s^{-1}$	19.91 ± 0.36	−13315.61 ± 28309.99	0.96
$10s^{-1}$	19.34 ±0 0.44	−14464.91 ± 37650.88	0.95
$100s^{-1}$	18.48 ± 0.51	−9101.94 ± 43074.99	0.96

This figure shows the positive and right-skewed distribution of the induction times, so it is taken that the data can behave as a Gamma, which is the distribution chosen for the data analysis.

Once the type of distribution and the order of the data have been chosen, the induction times are adjusted using a Gamma GLM. The summary of the coefficients of the different factors of the model is shown in Table 3. Taking into account the effects on the induction time utilizing the t-values, it can be observed that the temperature is the most influential factor, followed by gap, seed size and shear.

Lastly, diagnostic summaries were performed on the selected model. The deviance residuals of the model behave as a normal distribution, as shown in the Q-Q residuals plot in Fig. 8. A Shapiro-Wilk normality test on the deviance residuals also does not reject normalcy, with a p-value of 0.1432.

3.4. Cumulative distribution function

The variance of the induction time is very high, which could mean that the typical GLM analysis is not enough to study the induction times of xylitol crystallization. On the same token, these results are done using the classical nucleation theory, which is similar to a deterministic approach. However, crystallization can also be studied following the single nucleus mechanism, described in section 2.6.

For this study, all tests made at each temperature are grouped. For the fitting of the data, first, a linearization is done. Using equation (7), reordering the equation and taking the natural logarithm, one arrives at:

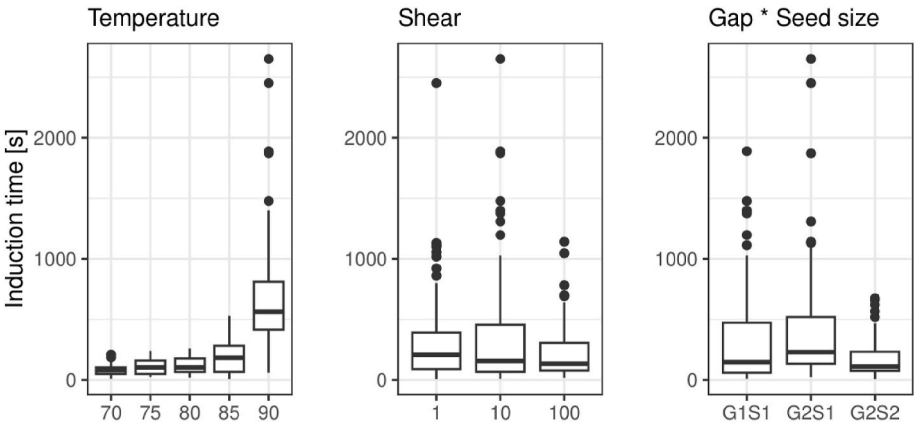

Fig. 6. Boxplot of induction times in seconds [s] by factor quantities: temperature (in °C), shear (in s^{-1}), and gap * seed size (in gap and seed size in μm; where G1S1: 600 μm//300 μm; G2S1: 1000 μm//300 μm; G2S2: 1000 μm//600 μm).

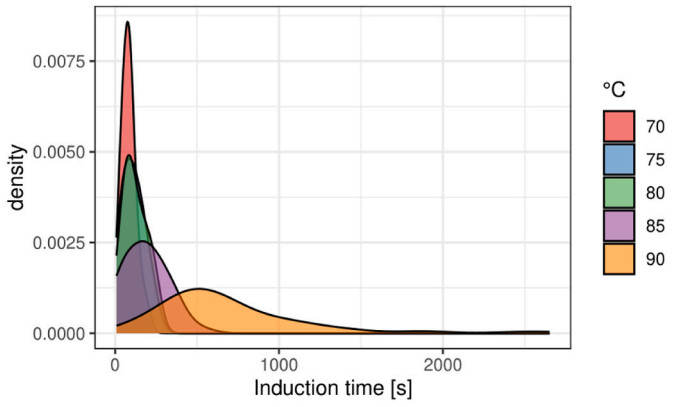

Fig. 7. Density distribution of induction time in seconds [s], by temperature quantities in [^{0}C].

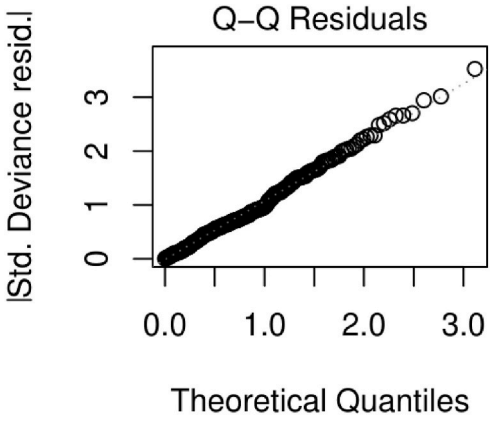

Fig. 8. Half-normal Q-Q plot of the absolute value of the standardized deviance residuals of the Gamma Generalized Linear Model.

Table 3
Estimated coefficients, t-values and p-values of the different factors used for the GLM.

Factor	Coefficient	t-value	p-value
1st order temperature	12.955	23.869	<2e-16
2nd order temperature	5.156	9.419	<2e-16
3rd order temperature	2.081	3.796	0.000182
Shear	−0.00184	−2.185	0.0298
Gap	0.00171	8.401	2.81e-15
Seed size	−0.00215	−6.891	4.09e-11

$$P(t) = 1 - \exp\left(-J \cdot V \cdot \left(t - t_g\right)\right) \rightarrow 1 - P(t) = -\exp\left(-J \cdot V \cdot \left(t - t_g\right)\right) \rightarrow \ln(1 - P(t)) = -J \cdot V \cdot t + J \cdot V \cdot tg \approx y = -m \cdot x + c \quad (8)$$

Where y, the dependent variable, is the natural logarithm of one minus the probability of a nucleus appearing, m, the slope, is the nucleation rate times the volume; x, the independent variable, is the induction time, and c, the independent term, is equal to the slope multiplied by the time delay for crystal detection.

The nucleation rate can be calculated by fitting the data to a straight line using the experimental data and knowing the sample volume (a cylinder with a radius of 2 cm and height of 600–1000 μm). Then, the nucleation rates can be compared to the ones calculated using the classical nucleation theory, shown in the next section. The results of the model are shown in Table 4.

Fig. 9 shows the cumulative probability of crystallization at different temperatures. As supercooling is higher, the induction times are reduced. However, in a storage system application, higher supercoolings lead to losses in the total energy stored, as shown in Navarro et al. [11].

Table 4
Nucleation rate and time delay results from the Poisson distribution model.

Temperature [^{0}C]	Nucleation rate (J [*/s·m^3])	Time delay (t_g[s])	R^2
70	26739.43	35.26	0.71
80	16539.84	45.39	0.86
90	2721.34	201.93	0.92

From Fig. 9, it can be observed that the difference in induction times at different temperatures is not linear. In a real system, part of the energy is lost due to recalescence, so some energy is lost as the supercooled material heats up to its melting point. Then, the energy storage system should be operated at temperatures lower than 90^{0}C, but without being too low as to lose a higher amount of energy. For example, at 80^{0}C, much shorter induction times are achieved in exchange for losing only 5 % of the energy [11].

3.5. Comparison between CNT and cumulative probability

Using the parameters obtained from equation 8, the different values of the nucleation rate and the minimum detection time are obtained, shown in Table 5. The CNT model does not consider the minimum detection time, so the comparison between the models is done only using the nucleation rate parameter.

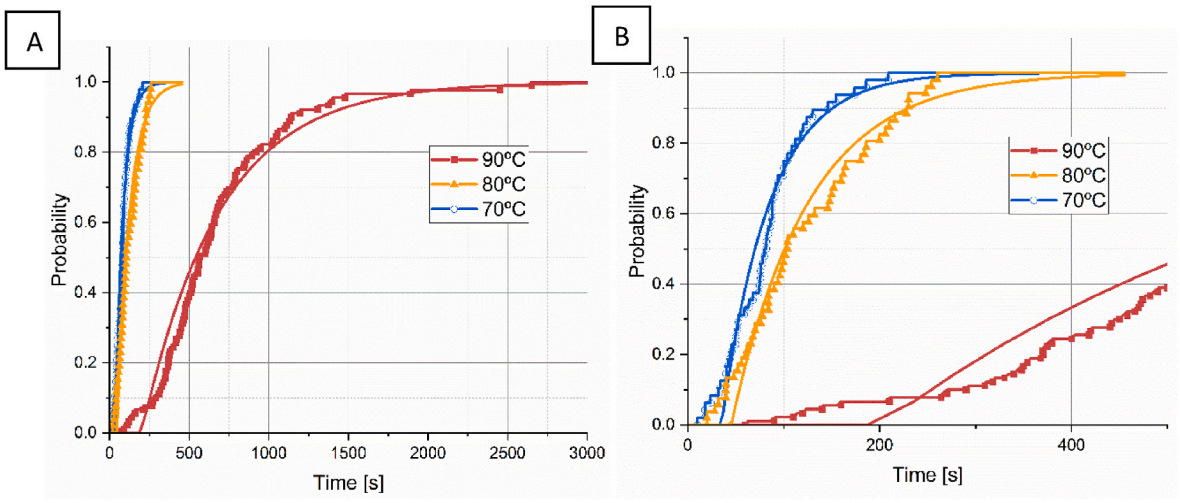

Fig. 9. A) Cumulative probability of crystallization. B) Zoom in the left part of the cumulative distribution function.

Table 5
Comparison between nucleation rates obtained from the Poisson distribution and the minimum nucleation rate obtained using the classical nucleation theory.

Temperature [^{0}C]	Nucleation rate (Poisson dist.) [*/s·m^3]	Nucleation rate (CNT) [*/s·m^3]
70	$2.64{\cdot}10^4$	$1.31{\cdot}10^6$
80	$1.65{\cdot}10^4$	$3.11{\cdot}10^6$
90	$2.72{\cdot}10^3$	$8.12{\cdot}10^3$

Even though the data is not disaggregated, the minimum nucleation rate obtained using the CNT at 70, 80 and 90 ^{0}C is higher than using the cumulative probability approach. This result is in line with the literature [18,22]. This comparison can be seen in Table 5.

4. Conclusions

In this work, the crystallization of xylitol by shearing and seeding has been studied using the viscosity-time curves obtained in rheometer tests. These tests have been carried out under different conditions of temperature, shear, gap and seed size. From each test, an induction time has been calculated, allowing crystallization to be analyzed from different perspectives.

The first approach has been to model the crystallization by classical nucleation theory, previously used in the literature to study the crystallization of xylitol [10]. This model does not fit well with the experimental results due to the large variation of the induction times and the unreliability of the model when trying to model a stochastic behavior by a deterministic model.

The second approach involves a statistical analysis of induction times. Due to the non-normality and large variance of the data, a generalized linear model adjusted to a gamma distribution was chosen.

Both the classical nucleation theory and the statistical analysis indicate that temperature is the most influential factor, followed by gap, seed size, and finally shear. Although shear may initially be considered a key factor affecting crystallization, its influence in this case appears to be limited, likely due to the difficult placement of the seed in the sample, as well as the variable shear rate when using a plate as geometry in the rheometer. It is recommended that the methodology is revised to better study this influence.

On the other hand, the cumulative distribution function of the induction times has been created by grouping the data by temperature. By fitting this function to a Poisson distribution, the nucleation rates have been calculated and compared with the calculated minimums of the CNT. It has been observed that these values are lower than the minimum calculated by the CNT, indicating that the CNT significantly overestimates the crystallization process.

Considering the results and the implications for a large-scale thermal energy storage system, it is advisable to penalize the temperature to achieve shorter induction times (accelerating the crystallization) until they become adequate for the intended application. However, supercooling causes the loss of part of the energy stored by the recalescence of xylitol. For an initial xylitol temperature of 80 °C, approximately 5 % of the energy is lost [11]. Nonetheless, at this temperature, the induction time is 250 s or less with a 95 % probability. Under the same probability, the induction time at 90 °C is 1500 s or less, which represents a sixfold increase in induction time. However, it should be noted that, although crystallization is slower at 90 °C than at 80 °C, the use of the seeding and shearing technique considerably accelerates crystallization in xylitol, even at low supercoolings [4].

Based on these results, scaling up the system to a stirred tank with seeding appears to be a promising approach, as it is expected to enhance the crystallization process. Additionally, the scaled-up system would provide an improved setup to investigate the effect of shear rate on the crystallization process.

CRediT authorship contribution statement

Miguel Navarro: Writing – review & editing, Writing – original draft, Visualization, Validation, Software, Methodology, Investigation, Formal analysis, Data curation, Conceptualization. **Zeus Gracia:** Writing – review & editing, Writing – original draft, Software, Methodology, Investigation, Data curation. **Jesús Asín:** Visualization, Validation, Supervision, Formal analysis, Conceptualization. **Ana Lázaro:** Writing – review & editing, Validation, Supervision, Resources, Project administration, Investigation, Funding acquisition, Formal analysis, Conceptualization. **Marta Martí:** Investigation, Data curation. **Mónica Delgado:** Writing – review & editing, Validation, Supervision, Methodology, Investigation, Formal analysis, Conceptualization.

Declaration of competing interest

The authors declare that they have no known competing financial interests or personal relationships that could have appeared to influence the work reported in this paper.

Acknowledgements

This work has been partially financed by the State Research Agency (SRA) and European Regional Development Fund (ERDF). Research

Projects: PID 2020-115500RB-I00, PID2023-148958OB-C21, TED2021-131061B–C31. Grant PRE2021-097131 funded by MICIU/AEI/10.13039/501100011033 and, as appropriate, by "ERDF A way of making Europe", by "ERDF/EU", by the "European Union" or by the "European Union Next Generation EU/PRTR" The with the additional support of the government of Aragon (Spain) (Reference group T55_20 R). Mónica Delgado thanks grant RYC2023-044207-I funded by.

MICIU/AEI/10.13039/501100011033 and the European Social Fund Plus.

(FSE+). Jesús Asín y Zeus Gracia Tabuenca were supported by Gobierno de Aragón (E46-23R) and Ministerio de Economía y Competitividad (RED2022-134202-T Biostatnet).

Data availability

Data will be made available on request.

References

[1] E.P. del Barrio, et al., Characterization of different sugar alcohols as phase change materials for thermal energy storage applications, Sol. Energy Mater. Sol. Cell. 159 (2017) 560–569, https://doi.org/10.1016/j.solmat.2016.10.009, ene.

[2] H.H. Zhang, et al., Experimental and in silico characterization of xylitol as seasonal heat storage material, Fluid Phase Equilib. 436 (mar. 2017) 55–68, https://doi.org/10.1016/j.fluid.2016.12.020.

[3] G. Diarce, A. Rojo, L. Quant, L. Bouzas, y A. García-Romero, Thermal endurance of xylitol as a phase change material for thermal energy storage applications, J. Energy Storage 55 (nov. 2022) 105717, https://doi.org/10.1016/j.est.2022.105717.

[4] M. Delgado, M.A.E. Navarro, A. Lázaro, S.A.E. Boyer, Edith Peuvrel-Disdier, y E. Peuvrel-Disdier, Triggering and acceleration of xylitol crystallization by seeding and shearing: rheo-optical and rheological investigation, Sol. Energy Mater. Sol. Cell. 220 (2021) 110840, https://doi.org/10.1016/j.solmat.2020.110840.

[5] S. Ur-Rehman, Z. Mushtaq, T. Zahoor, A. Jamil, y M.A. Murtaza, Xylitol: a review on bioproduction, application, health benefits, and related safety issues, Crit. Rev. Food Sci. Nutr. 55 (n.o 11) (2015) 1514–1528, https://doi.org/10.1080/10408398.2012.702288, abr.

[6] G. Galán, M. Martín, y I.E. Grossmann, Integrated renewable production of sorbitol and xylitol from switchgrass, Ind. Eng. Chem. Res. 60 (n.o 15) (2021) 5558–5573, https://doi.org/10.1021/acs.iecr.1c00397, abr.

[7] S.S. Queiroz, F.M. Jofre, S.I. Mussatto, y M.D. G.A. Felipe, Scaling up xylitol bioproduction: challenges to achieve a profitable bioprocess, Renew. Sustain. Energy Rev. 154 (feb. 2022) 111789, https://doi.org/10.1016/j.rser.2021.111789.

[8] M.L. Wolfrom y E.J. Kohn, Crystalline xylitol, J. Am. Chem. Soc. 64 (n.o 7) (jul. 1942), https://doi.org/10.1021/ja01259a509, 1739-1739.

[9] A. Godin, M. Duquesne, E.P. del Barrio, F. Achchaq, y P. Monneyron, Bubble agitation as a new low-intrusive method to crystallize glass-forming materials, Energy Proc. 139 (dic. 2017) 352–357, https://doi.org/10.1016/j.egypro.2017.11.220.

[10] Louis Piquard, Emilie Gagnière, Grégory Largiller, Denis Mangin, y F. Bentivoglio, Xylitol used as phase change material: nucleation mechanisms of the supercooling rupture by stirring, J. Energy Storage 48 (2022), https://doi.org/10.1016/j.est.2021.103922, 103922-103922, abr.

[11] M. Navarro, G. Diarce, A. Lázaro, A. Rojo, y M. Delgado, Comparative study on bubbling and shearing techniques for the crystallization of xylitol in TES systems, Results Eng. 17 (mar. 2023) 100909, https://doi.org/10.1016/j.rineng.2023.100909.

[12] A. Seppälä, A. Meriläinen, L. Wikström, y P. Kauranen, The effect of additives on the speed of the crystallization front of xylitol with various degrees of supercooling, Exp. Therm. Fluid Sci. 34 (n.o 5) (jul. 2010) 523–527, https://doi.org/10.1016/j.expthermflusci.2009.11.005.

[13] R. Bayón, R. Bayón, y E. Rojas, Feasibility study of D-mannitol as phase change material for thermal storage 5 (3) (may 2017) 404–424, https://doi.org/10.3934/energy.2017.3.404.

[14] X.-F. Shao, et al., Screening of sugar alcohols and their binary eutectic mixtures as phase change materials for low-to-medium temperature latent heat storage. (I): non-isothermal melting and crystallization behaviors, Energy 160 (oct. 2018) 1078–1090, https://doi.org/10.1016/j.energy.2018.07.081.

[15] I.M. Krieger y T.J. Dougherty, A mechanism for non-Newtonian flow in suspensions of rigid spheres, Trans. Soc. Rheol. 3 (n.o 1) (mar. 1959) 137–152, https://doi.org/10.1122/1.548848.

[16] H.M. Omar, y S. Rohani, Crystal population balance formulation and solution methods: a review, Cryst. Growth Des. 17 (7) (jun. 2017) 4028–4041, https://doi.org/10.1021/acs.cgd.7b00645.

[17] A.F. Izmailov, A.S. Myerson, y S. Arnold, A statistical understanding of nucleation, J. Cryst. Growth 196 (n.o 2) (1999) 234–242, https://doi.org/10.1016/s0022-0248(98)00830-6, ene.

[18] G.M. Maggioni, M. Mazzotti, y Marco Mazzotti, Stochasticity in primary nucleation: measuring and modeling detection times, Cryst. Growth Des. 17 (n.o 7) (jun. 2017) 3625–3635, https://doi.org/10.1021/acs.cgd.6b01781.

[19] G.M. Maggioni, M. Mazzotti, y Marco Mazzotti, Modelling the stochastic behaviour of primary nucleation, Faraday Discussions 179 (jun. 2015) 359–382, https://doi.org/10.1039/c4fd00255e.

[20] P.K. Senapati, B.K. Mishra, y A. Parida, Modeling of viscosity for power plant ash slurry at higher concentrations: effect of solids volume fraction, particle size and hydrodynamic interactions, Powder Technol. 197 (n.o 1–2) (2010) 1–8, https://doi.org/10.1016/j.powtec.2009.07.005, ene.

[21] B.J. Konijn, O.B.J. Sanderink, y N.P. Kruyt, Experimental study of the viscosity of suspensions: effect of solid fraction, particle size and suspending liquid, Powder Technol. 266 (nov. 2014) 61–69, https://doi.org/10.1016/j.powtec.2014.05.044.

[22] C. Brandel y J.H. ter Horst, Measuring induction times and crystal nucleation rates, Faraday Discuss 179 (2015) 199–214, https://doi.org/10.1039/C4FD00230J.

[23] C. Truong, L. Oudre, y N. Vayatis, Selective review of offline change point detection methods, Signal Process. 167 (feb. 2020) 107299, https://doi.org/10.1016/j.sigpro.2019.107299.

[24] A.M. Omran y C.J. King, Kinetics of ice crystallization in sugar solutions and fruit juices, AIChE J. 20 (n.o 4) (jul. 1974) 795–803, https://doi.org/10.1002/aic.690200422.

[25] A.S. Myerson, D. Erdemir, y A.Y. Lee (Eds.), Handbook of Industrial Crystallization, 3, Cambridge University Press, 2019, https://doi.org/10.1017/9781139026949 a.

[26] D. Kashchiev, Nucleation: Basic Theory with Applications, Butterworth Heinemann, Oxford, 2000.

[27] fourth ed., in: J.W. Mullin (Ed.), Crystallisation, 6, Butterworth Heinemann, Oxford, UK, 2001, pp. 201–202, https://doi.org/10.1021/op0101005, 600 pp. £75.00. ISBN 075-064-833-3.», Org. Process Res. Dev., mar. 2002, n.o 2.

[28] A. Mersmann, Supersaturation and nucleation, Chem. Eng. Res. Des. 74 (1996) 812–820.

[29] S. Jiang, y J.H. ter Horst, Crystal nucleation rates from probability distributions of induction times, Cryst. Growth Des. 11 (n.o 1) (2011) 256–261, https://doi.org/10.1021/cg101213q, ene.